# *Chapter V*

## Surface-wettability and structural colouration property of naturally occurring soft matter: flower petals (*Indian Rosacea*)

In plant kingdom, among flowers, *Rosaceae* (rose family) finds a distinct place not only by virtue of its brilliant appearance but also due to its placid fragrance, while captivating the attention of many bystanders. In the recent past, the bright colours and diverse varieties of roses have stimulated research interest to explore the underlying phenomena in these delicate specimens. With a biochemical perspective, the pigmentary or chemical colours have been extensively studied in naturally occurring species and it was found that, the colours due to these macromolecular constituents are generally dull, owing to the absorption of only certain wavelengths of light [1,2]. In contrast, the structural colour arises as a result of highly select microstructural make-ups, which largely dictate the surface feature of the specimen under consideration. In other words, patterned surfaces and sub-surfaces normally participate in structural colouration by way of numerous light scattering events at appropriate angles. There exist, numerous naturally occurring photonic structures which display tuneable structural colour [3]. The examples include, but not limited to butterflies, bird feathers, beetles, insects and flower-bearing plants [4-10]. Recently, the hyperfine ultrastructure of *Trogonoptera Brookiana* studied by Han *et.al* gave indication that these structures are sensitive to liquid medium [11]. While viewing under 3D microscope, the authors also witnessed the discolouration effect of the scales in response to the liquid medium. The bright, iridescent colour normally occurs in the nanoscale architecture of confined geometry, which is capable of producing a narrow-band spectral purity but of ultrahigh reflectivity [1].

On the other hand, the wetting-dewetting property of natural specimens is a vital aspect which helps in predicting the physiological state and environmental stability at large. The lotus (*Nelumbo Nucifera*) and toru (*Colocacia Esculenta*) leaves are excellent examples of non-sticky, super-hydrophobic surfaces that allow water droplets to roll off easily (water contact angle, CA $>150^{o}$) [12]. The super-hydrophobic surfaces exhibit excellent water repellency and are obvious choices for self-cleaning action. As regards wettabilityproperty

and structural colour, independent studies have been made previously on different rose varieties along with the characteristic *rose-petal* effect [1,12,13]. However, a qualitative account connecting wettability and structural colouration of these soft, delicate specimens has not yet been addressed. Furthermore, the colour-spread in the chromaticity diagram before and after chemical processing is rarely discussed in the literature. In this backdrop, the *Chapter V* is a detailed discussion as regards, comparative views on microstructural make-ups, reflectance responses and wettability features of certain rose cultivars belonging to *Indian Rosaceae* family and with off-to-dark pink appearances.

### 5.1 Specimen collection and processing

The specimens opted for our work were three varieties of the *Rosaceae* cultivars, namely, white rose (*Rosa chinensis var spontanea*), light pink rose (*Rosa chinensis var minima*), and dark pink rose (*Rosa chinensis var minima*). They are labelled as, W, LP and DP; respectively. To retain surface property, specimens were generally collected prior exposure to direct sun light. Accordingly, fresh flower specimens were gently collected from the plants available in our university garden during morning hours. Moreover, in order to retain the physiological state intact, the time gap between the plucking of flower and actual experiment was kept small (< 60 min), for every sample. The average dimension of the petals examined varied in the range of 12 mm x 25 mm. In order to exploit the nature of discolouration effect, each of the specimens is treated with ethanol, propanol and glycerine separately (Fig. 5.1(A)).

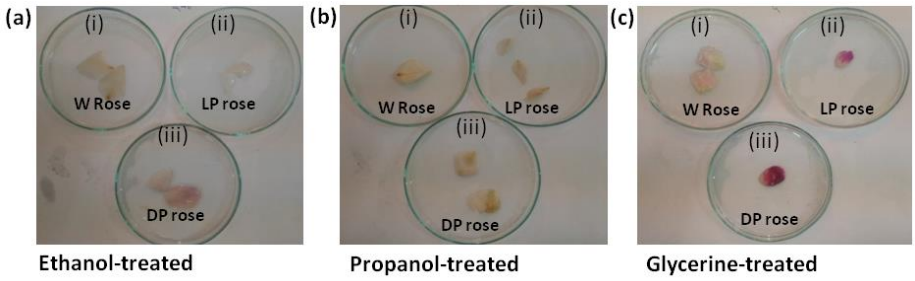


Figure 5.1: White (W), light pink (LP) and dark pink (DP) rose petals each of which is treated with (a) ethanol, (b) propanol and (c) glycerine independently.

## 5.2 Micro-morphological analysis of the rose petals

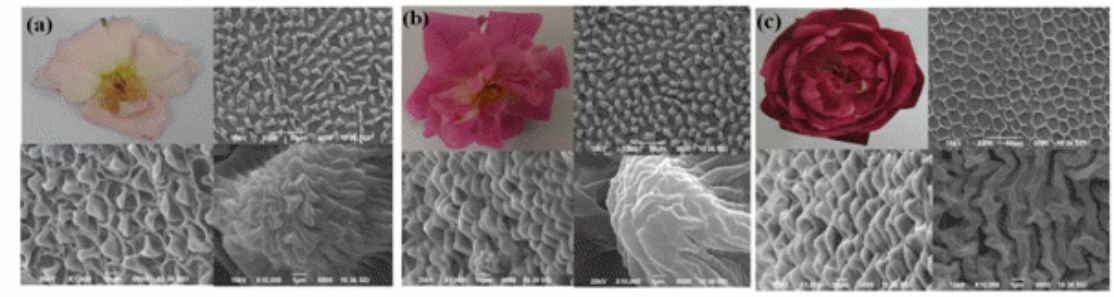


Figure 5.2: SEM images of the three varieties of *Rosaceae* cultivars: (a) white rose, W (b) light pink rose, LP and (c) dark pink, DP rose petals. The upper left corner depicts digital snapshots of the rose specimens, whereas upper right corner highlights microscopic distribution of micro-papillae assembly in each case. The lower panels illustrate scanning electron micrographs captured at higher magnifications. Note the dimension and orientation of the micro-papillae along with nano-folders within single micro-papillae.

The digital snap-shots as well as SEM micrographs (captured at different magnifications) of the white (W), light pink (LP) and dark pink (DP) roses are depicted in Figure 5.2(a-c). While the appearance of flowers clearly illustrates varied colour strength, the micrographs showed numerous micro-papillae assemblies with varying dimension, orientation and folds. The presence of micro-papillae, essentially the papillae on the rose petals appear with circular wrinkles or folds, are mainly responsible for enhancing the surface roughness of the petals [14]. Each of the papillae, essentially comprises of single cells, and therefore, every petal would comprise of several thousands of these micro-papillae. Furthermore, the magnified SEM images depict the presence of nano-folders and nano-binders within each papillae. Even though each of the micro-papillae varies in dimension, distribution and orientation they exist in isolation from each other.

Microscopically, the white rose petals signify aperiodic distribution of the oblate to conical units at large (Figure 5.2(a)). The light-pink petals, however, give a better homogeneity in terms of microscopic distribution of the oblate units while they differ in dimension and tilt (Figure 5.2(b)). As a result, the LP

Table 5.1: Physical parameters of the *Rosacea* specimens under study

| **Specimen** | **Approximate base-width of the micro-papillae, *d* (μm)** | **Height of the micro-papillae, *h* (μm)** | **Aspect ratio, $A_r$** | **Micro-papillae peak-to-peak distance (μm)/ pitch (*p*)** | ***p/h*** |
|---|---|---|---|---|---|
| White rose (W) | 11.06±4.6 | 12.80±6.5 | 1.16 | 15.95±6.1 | 1.25 |
| Light pink rose (LP) | 9.78±3.6 | 9.57±4.5 | 0.97 | 15.20±4.1 | 1.58 |
| Dark pink rose (DP) | 12.0±4.5 | 12.65±4.8 | 1.04 | 15.67±4.6 | 1.23 |

rose petals can have a relatively more unfilled space within its surface structure. In contrast, the DP rose petal possesses round shaped micro-papillae, which gives an impression of the cage-like network (Figure 5.2(c)). Nevertheless, the W and LP rose specimens possess short, elongated micro-papillae packed loosely or tightly at the surface site. However, the periodic arrays of nanoscale entities within the micro-papillae systems resemble photonic crystal structure, and might contribute considerably to the iridescence feature. The DP specimen, owing to its spectacular, periodic morphological micro-papillae assembly would prohibit surface scattering events, to a great extent, giving off deep, dark pink colour. This kind of micro-morphological periodicity can also be apprehended in butterflies, beetles, insect etc. which were believed to be the primary sources of iridescent structural colour [15]. A side view of the nano-folders and nano-oblates can be clearly seen at a higher magnification, for each rose-petal types. The physical parameters as regards, micro-papillae size, distribution etc. were determined directly from the micrographs by employing *ImageJ*® [16] software and can be found in Table 5.1.

## 5.3 Surface wettability property of the rose petals

### 5.3.1 Model on micro-papillae assembly and theoretical treatment

Two well accepted models are generally employed to describe wetting-dewetting phenomena: Cassie-Baxter (C-B) and Wenzel models [17, 18]. As discussed earlier, the C-B model describes the suspended state of the liquid

droplet, whereas, the Wenzel model accounts for the collapsed state as the placement of water droplet allows to fill up the grooves completely. The CA of water droplet on any rough surface is mainly described by Wenzel and C-B model, the relevant equations being described in earlier chapters.

It is known that, surface roughness and chemical composition both play dominant roles for displaying hydrophobicity [19]. While assessing wettability features, CA hysteresis (CAH) describes an important parameter for examining (high or low) surface adhesion to water, especially for the hydrophobic surfaces [20]. Thus the determination of CAH is an important aspect while evaluating hydrophobic/ hydrophilic nature of the surface structure. In this regard, tilted plate methodology is a versatile and proven technique for exploiting the advancing (max.) and receding (min.) contact angles of the water droplet on a given surface under study and measured for different tilting angles [21]. As regards, CAH, two modes are already in place: *rose-petal effect* and *lotus effect*. Generally, a low hysteresis value indicates low solid-liquid adhesion, and a high CA hysteresis signifies a high solid-liquid adhesion [22]. A surface which characterise high CA and high CAH is said to exhibit *rose-petal* effect, while the lotus effect is displayed by a surface that has high CA and low CAH [12]. To be precise, surface roughness mediated adhesion could affect CAH substantially and that, the pinning effect causes the droplet to stick to the surface. In this regard, being a unique surface phenomenon, the petal effect is characterized by a large CA, CAH and strong adhesion to water. A clear transition between the wetting regimes has already been predicted in earlier works [23,24]. Accordingly, different rose varieties can have petals with both high and low surface adhesion characteristics which are invariably dependent on their surface microstructure [23]. In reality, for a surface make-up with sub-micron or nanoscale protuberances in each of the micro-papillae, water is believed to get adsorbed into the pockets of the air gaps slowly while undergoing a continuous transition from de-wetting to wetting point [24].

In reference to schematic illustrations, shown in Figure 5.3(a, b), physical parameters that would help in determining wetting and de-wetting characteristics are: pitch value ($p$), diameter ($d$) and pitch-base height ($h$). The pitch value is defined as the average peak-to-peak distance between any two micro-papillae, whereas, pitch-base height represents the approximate height of the micro-papillae [24]. A smaller value of $p/h$ ratio applies to the C-B regime, which tends to increase the static water CA. This ratio is important in the sense that, a lower value enhances the formation of air-pockets between the microstructures, and consequently, the water droplet cannot come in contact with the bottom surface [24]. In other words, when the effective contact area between the water droplet and the microstructure is minimized, the static CA increases for surfaces with low adhesion. Undoubtedly, numerous factors are greatly responsible as regards hydrophobic feature of the surface make-up is concerned. For a water droplet of size comparable to the pitch value, liquid may penetrate deep inside the grooves, but if the droplet is large enough, then it will be supported only by the top surfaces of the pillars of the micro-papillae, thereby forming numerous air gaps beneath the droplet base [25]. Not surprisingly, for a surface with ample micro- and nanoscale roughnesses, the hydrophobicity is believed to be the outcome of the combined effect, though it is quite difficult to isolate individual contributions.

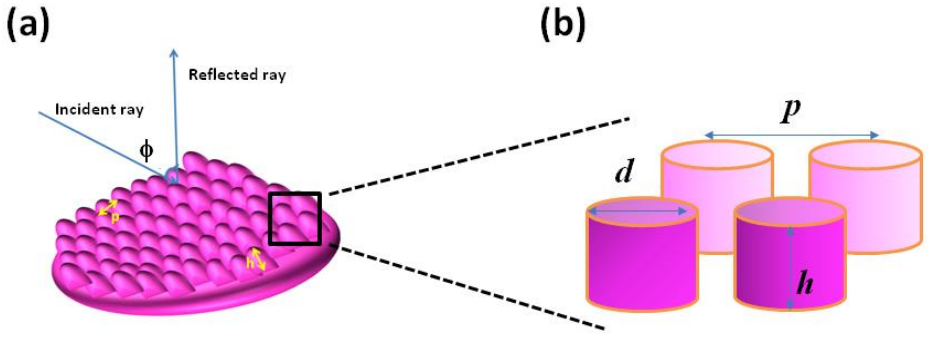


Figure 5.3: (a) Schematic representation of an assembly of micro-papillae within a rose petal along with light scattering aspect and (b) side view of four micro-papillae in a square area highlighting pitch and height of the micro-papillae.

For simplicity, the approximate microstructure roughness factor ($r_\varphi$) can be calculated by visualizing the micro-papillae as regular cylinders characterized by diameter ($d$), height ($h$) and pitch value ($p$) that can be found over a square area (Figure 5.3(b)). Here, the roughness factor, $r_\varphi$ is defined as the ratio of the actual, effective surface area ($A_{eff}$)to the projected, geometrical surface area ($A_{proj}$). In a square area of length equal to the pitch value, the projected surface area is, $p^2$; whereas actual area is the sum of the curved surface area of the cylinder and the exposed surface area.

To a good approximation, the actual surface area can be written as, $p^2+\pi dh$. Therefore, for a cylindrical system with its top being in contact with the water droplet [23],

$$r_\varphi = A_{eff}/A_{proj}$$

or,
$$r_\varphi = \frac{p^2+\pi dh}{p^2}$$

$$r_\varphi = 1 + \frac{\pi dh}{p^2} \qquad (5.1)$$

And the fraction of the solid-liquid contact under the droplet that would participate in the wetting de-wetting transition can be expressed as,

$$\varphi = \frac{\pi d^2}{4p^2} \qquad (5.2)$$

Combining the above two relations, one can interrelate surface roughness with the fractional solid-liquid contribution given as,

$$\varphi = \frac{d}{4h}(r_\varphi - 1) \qquad (5.3)$$

The aforesaid parameters predicted for the rose petals under study are enlisted in Table 5.1 and 5.2.

### 5.3.2 Experimental features on wetting-dewetting transition

The static CA features of the three varieties of the rose petals are shown in Figure 5.4 (a-c) and Table 5.2. The shape of the water droplets at a base-tilting of 0 and 90$^o$ are depicted in Fig. 5.4 (a-c). The curves representing advancing (max.) and receding (min.) CA with varying tilting angles as well as CA

hysteresis traces can be found in Fig. 5.5 (a-d). The petal surfaces are essentially hydrophobic with a maximal CA exhibited by the DP petals at a higher tilting angle. As can be noticed, the DP rose petals offer a superbly high CA and a large $r_\varphi$ value owing to a comparatively lower *p/h* ratio (Table 5.1 and 5.2). To be specific, in this case, $r_\varphi$ =2.94 and $\varphi$ = 0.46. Amongst all, the off pink, LP rose petals offered comparatively low values of wetting-dewetting parameters, with $r_\varphi$ = 2.27 and $\varphi$ = 0.32. In fact, a higher value of the roughness factor is likely to improve surface hydrophobicity with marginal enhancement in the solid-water fraction as per equation (5.5). Apparently, an improved CA, high CAH and large $r_\varphi$ values are mainly responsible for displaying enhanced hydrophobic features. On the other hand, the water droplet may develop a tendency to impregnate into the grooves for a moderate rough surface. In contrast, a different correlation has been found in insect systems, such as, damsel and dragonfly wings [26].

Wetting transition is an important mechanism which needs to be understood for the development of super-hydrophobic surfaces artificially. Normally, a particular system has a single, Young's CA value, relevant for a genuinely smooth surface structure. But one could observe altered CA values due to a variation in the local geometrical construction between any two sites. It has been explained theoretically that, the Gibbs free energy of a system can have multiple minima and a single global minimum. Each of the CA value corresponds to the

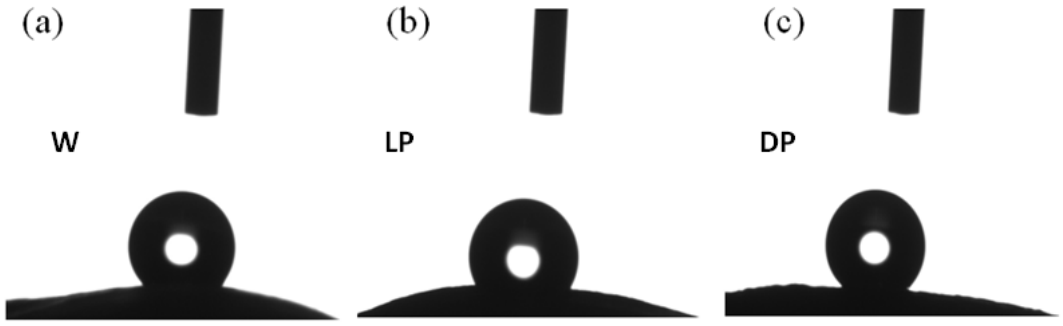


Figure 5.4: Static water contact angle (CA) values measured on flat surfaces of (a) white, (b) light pink, and (c) dark pink rose petals.

metastable state of the system and the global equilibrium is given by the so-called most stable CA [21]. We have measured the advancing (max.) and receding (min.) CA for every unit degree of base-tilting, while moving from 0 to 90° (Figure 5.6(a-d)). With tilting progression, certain critical angles ($\alpha$) are defined at which the drop tends to slide. The angles at which the first displacement of the contact line occurs and the angle for which both the uphill and downhill contact line displaces are termed as critical angles [27]. The observed critical tilt angles are predicted as, 18° for the W rose; 29° and at 57° for the LP rose; and 18° and 39° for the DP rose petals. The parameters as regards, CAH, critical angle and surface energy can be found in Figure 5.6 (a-d) and Table 5.2.

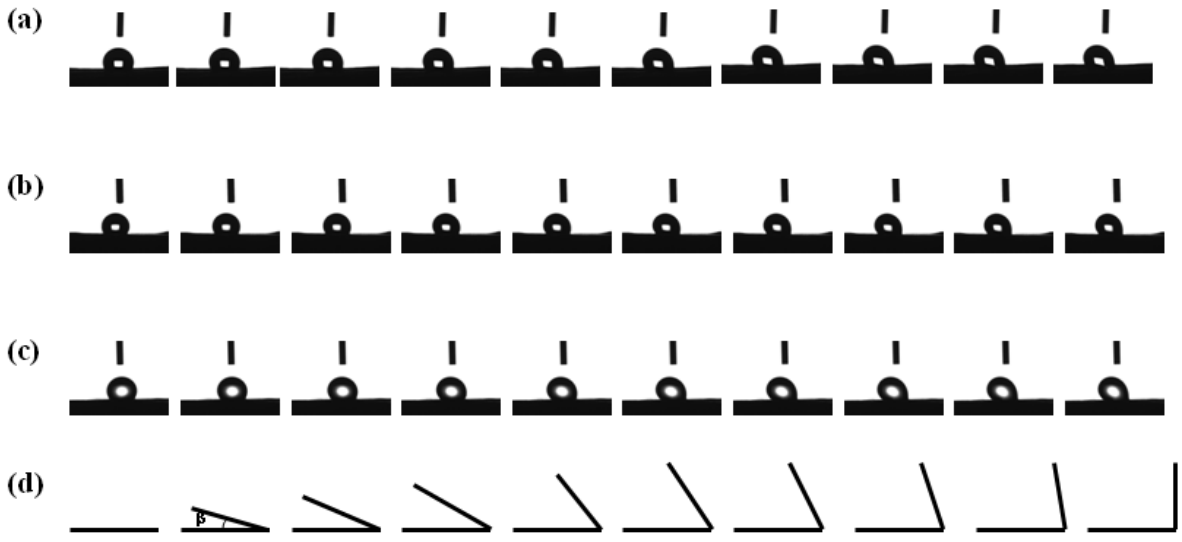


Figure 5.5: The measured CA in tilting base methodology, corresponding to a base tilting of $0^0$ to $90^0$ in steps of $10^0$; respectively.

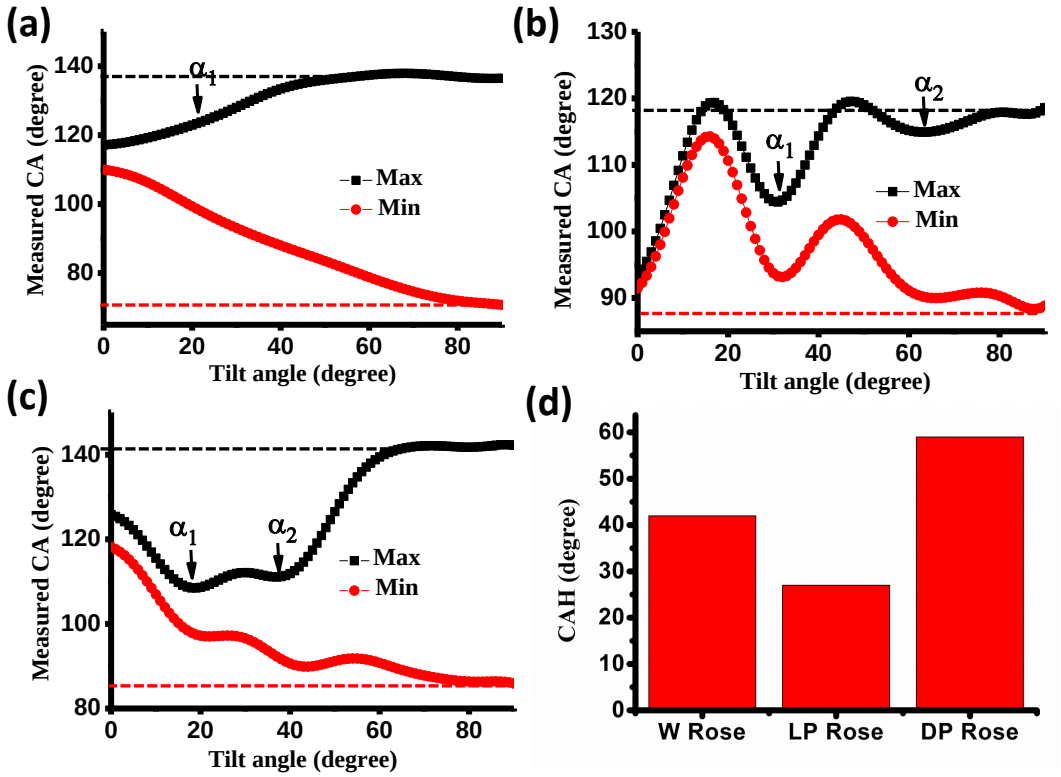


Figure 5.6: Advancing (maximum) and receding (minimum) contact angles measured in tilting base methodology as for (a) white (W), (b) light pink (LP), and (c) dark pink (DP) rose petals. The histograms depicting CAH for the three samples are shown in (d).

Table 5.2: Measured parameters related to dewetting phenomena on the rose-petal

| Sample | Bump density (1/10,000 $\mu m^2$) | Static CA (deg.) | Roughness factor, $r_\varphi$ | Solid-water fraction, $\varphi$ | Advancing and receding CA (deg.) | Transitional roughness, $r_t$ | CAH (deg.) | Critical angles, $\alpha_1$; $\alpha_2$ (deg.) | Surface energy (mJ/m$^2$) |
|---|---|---|---|---|---|---|---|---|---|
| White rose, W | 27 | 122.5±0.2 | 2.74 | 0.37 | 137; 86 | 1.23 | 51±0.31 | 18°; – | 49.8 |
| Light pink rose, LP | 33 | 111.2±0.2 | 2.27 | 0.32 | 117;90 | 1.83 | 27±0.27 | 29°; 57° | 152.8; 264 |
| Dark pink rose, DP | 24 | 133.3±0.2 | 2.94 | 0.46 | 142;83 | 1.15 | 59±0.33 | 18°; 39° | 13.1; 28.6 |

Here, we witnessed significant changes in advancing ($\theta_{adv}$) and receding ($\theta_{rec}$) angles, which are in consistency with the principle of the *petal effect*. Since the rose petals under study vary in surface structure, wetting-dewetting feature also changes as can be noticed by CA and CAH plots. The CAH essentially foretells the state of a liquid droplet, with small CAH representing the droplet in Cassie state. As the droplet is allowed to slide on a surface with the tilting angle from 0° - 90°, localized roughness is at work which prevents the droplet from rolling/rapid sliding. For a water droplet undergoing Wenzel mode, normally the CAH value tends to increase with increasing surface roughness [28]. In the C-B state, however, the CAH is largely influenced by the solid-liquid fraction. When the droplet undergoes sliding, it would certainly experience changes along smaller pockets in terms of roughness, causing changes in the shape and curvature of the droplet. This will certainly allow transition between the Cassie and the Wenzel states. As the droplet bends, it will develop a tendency to penetrate the empty space between the micropapillae, thereby increasing the difference between the CA maxima and minima. Revealing the CAH along with the static CA enhances our insight on the effect of microstructure on the water-repelling surfaces. The CAH influences the pinning of the droplet, which does not allow the droplet to roll off easily while retaining hydrophobicity at large. This is possible even if the base tilting reaches a maximal value of 90°. The pseudo super-hydrophobic nature of the rose petals and gecko feet has already been referred in literature [29, 30]. Not surprisingly, despite the hydrophobic nature of the surfaces, the droplets may not necessarily roll off owing to the pinning effect as predicted in earlier works [31].

The Wenzel and C-B model can be simultaneously applied to reveal the transitional roughness ($r_t$) at the transitional point [32], given by:

$$r_t = \frac{\varphi-(1-\varphi)}{\cos\theta_{adv}} \qquad (5.4)$$

with $\theta_{adv}$ as the equilibrium CA. The extrapolated black dotted line drawn from the saturation part of the advancing CA curve towards y-axis and the red dotted

line gives the receding angle (Fig. 5.6 (a-c)). The values of the transition point in the three rose varieties are listed in Table 2. For $r_\varphi < r_t$, the droplet penetrates into the grooves, and thus the specimen is likely to obey the Wenzel mode. Whereas, for $r_\varphi > r_t$, the droplet is said to be in Cassie state. Accordingly, the water droplets in the rose petals, follow Cassie state. While undergoing transition from the Wenzel to the Cassie state [32], significant changes in the $\theta_{adv}$ and $\theta_{rec}$ have been witnessed in all the three kinds of rose-cultivars.

## 5.4 Structural colouration in light-to-dark pink rose petals

### 5.4.1 Manifestation of reflectance features

The characteristic reflectance spectra of the three varieties of the rose specimens, namely white (W), light pink (LP) and dark pink (DP) studied with and without chemical treatment, are depicted in (Figure 5.7(a-c)). As for surface treatment, the matured petal specimens were dipped in three different liquids, namely ethanol (*RI*=1.36), propanol (*RI*=1.39) and glycerine (*RI*=1.47). The idea behind the liquid adsorption was to alter the micro-morphological features by varying

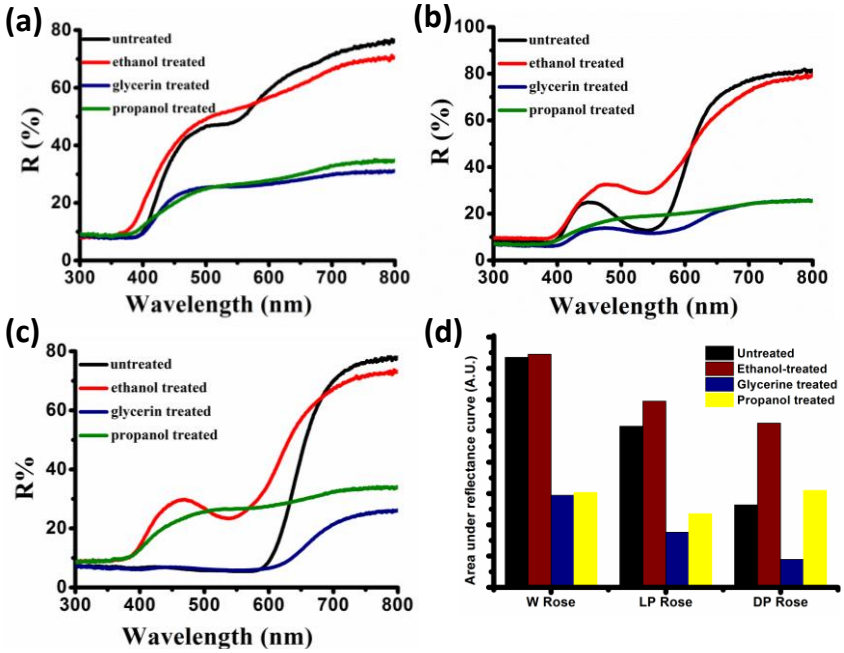


Figure 5.7: Reflectance spectra of three varieties of *Rosaceae* cultivars before and after liquid immersion: (a) white (W), (b) light pink (LP), and (c) dark pink (DP) rose petals.

the *RI* of the environment, which could bring in significant changes in the reflectance spectra. Earlier, the appearance of colour was believed to be caused by the change in the RI of the building elements or through transient modification in its dimensions [33]. The specimens offered either similar or different reflectance curves in a particular range of wavelength. Referring to W and LP petals, the former exhibited a steadily growing reflectance trend beyond 400 nm along with a broad peak observable at ~510 nm. Whereas, the LP specimen displays a distinct reflectance maximum located at ~455 nm and a dip at ~545 nm, beyond which reflectance curve has a growing trend. On the other hand, the DP specimen gives a poor reflectance up to ~590 nm, followed by a sharp rising trend afterwards. In other words, the petals of the dark pink rose are non-reflecting in a large part of the visible spectrum and thus would offer a dark impression to the unaided eyes. This is owing to intense light absorption in the most part of the visible wavelength range while excluding the orange-red part of the electromagnetic spectrum.

As can be noticed, the untreated specimen is highly reflective in the infra-red regime. Infact, all the specimens are highly reflective beyond red-part of the spectrum, but to different strengths. The insertion of these solvents with varying refractive indices into the air-pockets and sub- micron voids is likely to alter the RI of the petals as a whole. Note the modified reflectance curves (after liquid treatment) for W, LP and DP specimens (Fig. 5.7(a-d)). Each of the soaked petals gave distinctly different characteristics with the emergence or disappearance of peaks for a given specimen type. While ethanol dipped W rose petal, exhibited a similar, yet broadened reflectance feature in reference to the untreated one; propanol and glycerine treated W specimens provided significantly lowered reflectance features. Upon ethanol uptake, the LP rose petals gave a shifting of the reflectance peak from ~455 nm to 478 nm, however, the DP specimen offered the emergence of a new peak (located at ~465 nm), which was otherwise absent for the untreated case. As clearly seen from the reflectance curves of both the LP and DP specimens, the colour tends to fade

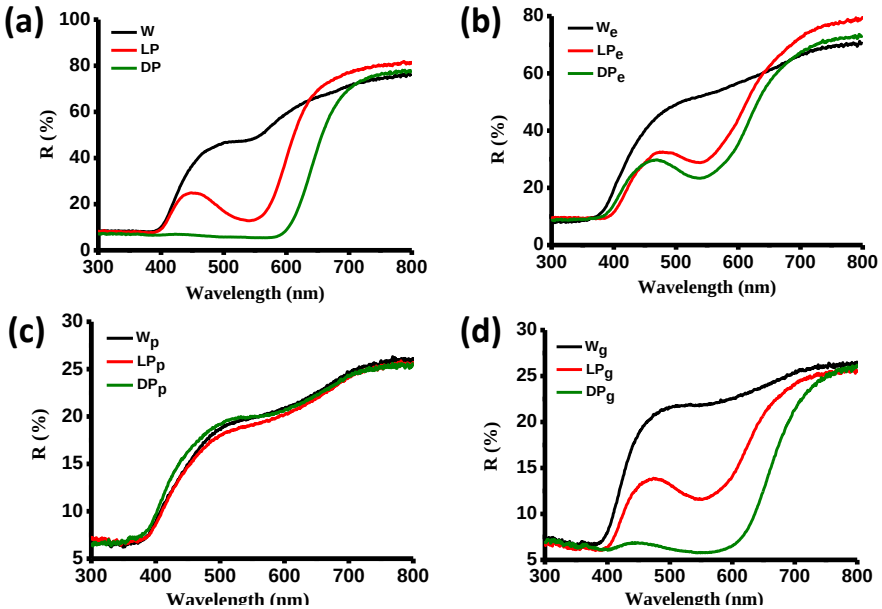


Figure 5.8: All the reflectance curves without and with liquid immersions are shown collectively in (a)-(d). The respective labels $W_e$, $LP_e$ and $DP_e$; $W_p$, $LP_p$ and $DP_p$ ; $W_g$, $LP_g$ and $DP_g$ represent specimens after ethanol, propanol and glycerine treatment.

away for the specimens immersed in the liquids of propanol and glycerine. In these cases, we could also witness bleached view of the petals through the unaided eyes. It is interesting to note that, geraniol, a mono-terpenoid and alcohol, which constitutes an important component of rose oil, has *RI*=1.46 in ambient environment. Most likely when voids are filled with glycerine, the whole specimen would behave as an entity dispersed in geraniol. As a result, structural contribution to colour is drastically suppressed and pigmentary contributions become more pertinent to colouration (Fig. 5.7(d)). Thus one can say that, a substantial difference in RI within the treated petals can be set by ethanol and propanol media (Fig. 5.8 (b) and (c)). To be specific, in case of ethanol treatment, one could realise a great similarity in the reflectance responses exhibited by the LP and DP petals. In contrast, after propanol uptake, all the specimens fade away giving similar reflectance trends (Fig. 5.8 (c)). These aspects are ascribed to the momentary structural resemblance in the aforesaid petals. Consequently, they signify suppression/removal of the dyes. Even though the colour that appears is a combined effect of pigmentary and

structural colour, the latter component gets altered once the RI of the environment is varied.

Since the bands are generally broad, with reflectance responses between any two specimens different, we intended to focus on the LP petals, which exhibited a clear peak shifting upon chemical processing. A simple relationship between the optical stop bands and the periodicity of the nano-structured pattern can be given by the Bragg's law [1]:

$$\lambda = 2d\, n_{eff}, \tag{5.5}$$

$$\lambda' = 2d\, n_{eff}' = 2d\,(n_{eff}+\Delta n) = 2d\, n_{eff}\left[1 + \frac{\Delta n}{n_{eff}}\right], \tag{5.6}$$

where, $n_{eff}$ is the effective *RI* of the system under study and $d$ is the period which is assumed to be unaltered before and after ethanolic adsorption. The respective *RI* of the air gap, geraniol, ethanol, propanol and glycerine are approximately, 1.0, 1.46, 1.36, 1.39, 1.47. Consequently, the $n_{eff}$ values are 1.23, and 1.27, 1.28 and 1.31; as for the untreated, and respective specimens treated with ethanol, propanol and glycerine. Here, many ultra-small air pockets are still assumed to remain unfilled even after the time necessary for complete liquid adsorption. This is because, diffusion, rapid evaporation, capillary mechanism and other surface-interface phenomena cannot be avoided completely.

Inserting $\lambda$=455 nm and $n_{eff}$ =1.23 in equation (5.4), we obtain $d$~185 nm. Apparently, this cannot be compared to the pitch of the micro-papillae which has micron scale dimension. However, the periodicity could be linked to the average repeat units of the nano-folders and air gaps that make up the micro-papillae (Fig. 5.3). On substituting the values, $d$~185 nm and $n_{eff}$ =1.27, 1.28 and 1.31 in equation (5.5), we obtain $\lambda'$ ~470, 474 and 485 nm as can be witnessed in the reflectance curves (Figure 5.7 and 5.8). It is, however, worth mentioning that, while the strength of reflectance is largely described through the surface microstructure, the wavelength at which most of the light is reflected has its origin on the conditions set by specular and diffuse scattering events. Earlier,

the peak maximum at a higher wavelength for the rose petals was ascribed to the collective contributions originated through microstructural arrangement and chemical pigments/species.

### 5.4.2 Chromaticity features – A comparative view

We have also translated the reflectance data into the chromaticity diagrams, employing CIE 1931 colour space [34]. Essentially, a chromatogram characterizes the loci of the wavelength reflected with different intensities, by converting the wavelength to the (x, y) coordinates, known as chromaticity coordinates. The chromaticity diagrams can be extremely useful as they are capable of identifying and assigning the exact colour of a given specimen in the colour space [34]. Such diagrams are extremely meaningful for describing coloured species including those of multi-coloured butterflies [34, 35]. The chromaticity diagrams for different rose petals can be found in Fig. 5.9 (a-d). Here, an arbitrary point on the line joining between any two apex colours would represents a proportionate mixture of those. The triangular gamut formed as a result of the line joining B, G and R depends on the choice of the focus with the centroid, identified as pure white ($W^*$). The white rose petals, without and with ethanol treatment, exhibited scattered points around $W^*$ with slight stretching along terminus R (Fig. 5.9(a), (b), col.1). However, a more precise accumulation of points within the central region along with directed extension towards R has been clearly witnessed in the LP specimen (Figure 5.9(a), col.2). Upon ethanol treatment, the points representing reflectance response around the central region is much scattered without loss of generality with respect to the untreated case. Nevertheless, the DP rose specimen gave a continuous stretch of the reflectance points from around the vicinity of $W^*$ to the R terminus (Figure 5.9(a), col.3). In other words, the dark appearance of DP specimen could be due to the dominance of R segment in the aligned gamut of the colour space. Upon ethanol uptake, the distribution of reflecting points of

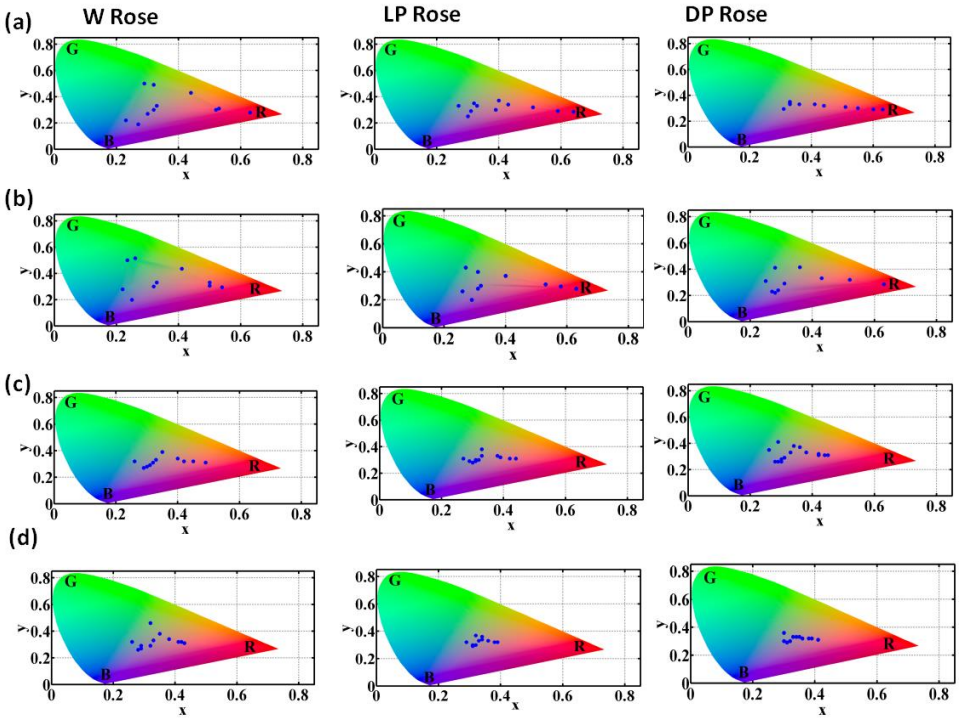


Figure 5.9: CIE chromaticity diagrams corresponding to the untreated white (W), light pink (LP), and dark pink (DP) rose petals are shown in (a) (col. 1, 2 and 3). The respective chromaticity features as for the ethanol, propanol and glycerine treated specimens are presented in rows (b), (c) and (d); respectively.

the DP specimen is more open at the centroid and the chromaticity pattern becomes largely similar as to the treated DP rose specimen (Fig. 5.9(b), col.2 and 3). At the microstructural level, both the LP and DP rose petals would share a common physical trend after the ethanol insertion. Accordingly, similar reflectance and chromaticity features have been ensured. This is, because, ethanol uptake is likely to cover up many of the rough surfaces by way of filling air pockets/voids available within and around the micro-papillae. It is worth mentioning here that, the visible light would experience adequate surface scattering from the bumpy assembly of the micro-papillae which essentially depends on varying *p/h* value. Moreover, a lowered bump density and pitch value in the DP petals ensure a stronger absorption response and consequently, a deep pink colour appears when viewed through the unaided eye. Moreover, the chromaticity diagrams, particularly for the propanol and glycerine treated

specimens (Figure 5.9(c), (d), col.2 and 3), exhibited apparent accumulation of points around the W*, thereby indicating colour fading in these cases asdiscussed above.

## 5.5 Conclusions

The cultivars of *Indian Rosaceae* family have been examined to exploit surface wettability and structural colouration characteristics. The surface roughness, $r_\varphi$ which is highly dependent on the nature of arrangement of micro-papillae with different *p/h* ratio plays an important role for displaying de-wetting feature. With a lowered pitch-to-height ratio, the DP rose petal exhibited maximal values of static CA (=133$^o$), $r_\varphi$ (=2.94) and CAH (=59$^o$). As compared to the other two varieties, the reflectance response of DP specimen is significantly lowered over the whole visible wavelength range. However, immersion in ethanol, propanol and glycerine could exhibit distinct roles for improving reflectance feature. In particular, a prominent reflectance peak appeared after ethanolic uptake. Moreover, the reflectance features of the LP and DP specimens after ethanol-treatment are quite similar owing to the establishment of a common micro-morphological and optical trend. Similarly, propanol treatment gave quite alike reflectance features, for all the rose cultivar kinds. The dimension and distribution of the micro-papillae or micro-bumps, were believed to influence the surface morphology profoundly. Connecting wettability with reflectance trend mediated via surface roughness characteristics would find scope in softonics by way of bridging soft matter physics and biophotonics at large.

## References

[1] Feng, L., Zhang, Y., Li, M., Zheng, Y., Shen, W., Jiang, L. The structural color of red rose petals and their duplicates. *Langmuir*, 26:14885-14888, 2010.

[2] Glover, B. J., Whitney, H. M. Structural colour and iridescence in plants: the poorly studied relations of pigment colour. *Annals of Botany*, 2010, 105, 505-511.

[3] Wang, Z. L. L., Guo, Z. G. Biomimetic Photonic Structures with Tunable Structural Colours: From Natural to Biomimetic to Applications. *Journal of Bionic Engineering*, 15:1-33, 2018.

[4] Vukusic, P., Sambles, J. R. Photonic structures in biology. *Nature*, 424:852-855, 2003.

[5] Vukusic, P., Sambles, J. R., Lawrence, C. R., Wootton, R. J. Structural colour: Now you see it — now you don't. *Nature*, 36:409-410, 2001.

[6] Vukusic, P., Sambles, J. R., Lawrence, C. R. Structural colour mixing in wing scales of a butterfly. *Nature*, 404:457, 2000.

[7] Zi, J., Yu, X., Li, Y., Hu, X., Xu, C., Wang, X., Liu, X., Fu, R. Coloration strategies in peacock feathers. *Proceedings of the National Academy of Sciences U.S.A.*, 100:12576-12578, 2003.

[8] Parker, A., Welch, V. L., Driver, D., Martini, N. Structural colour: opal analogue discovered in a weevil. *Nature*, 426:786-7, 2003.

[9] Parker, A., Mcphedran, R. C., Mckenzie, D. R., Botten, L. C., Nicorovici, N. A. Photonic Engineering. Aphrodite's iridescence. *Nature*, 409:36-7, 2001.

[10] Kinoshita, S., Yoshioka, S. Structural colors in nature: the role of regularity and irregularity in the structure. *ChemPhysChem,* 6:1442-1459, 2005.

[11] Han, Z. W., Yang, M., Li, B., Mu, Z., Niu, S. C., Zhang, J. Q., Yang, X. Excellent Color Sensitivity of Butterfly Wing Scales to Liquid Mediums. *Journal of Bionic Engineering*, 13:355-363, 2016.

[12] Nosonovsky M, Bhushan, B. (eds.) *Green Tribology, Green Energy and Technology*, Springer-Verlag, Berlin, Heidelberg, 2012.

[13] Feng L, Zhang Y, Xi J, Zhu Y, Wang N, Xia F, Jiang L. Petal Effect: A Superhydrophobic State with High Adhesive Force. *Langmuir*, 24, 4114-4119, 2008.

[14] Ebert, D., Bhushan, B. Wear- resistant rose-petal effect surfaces with superhydrophobicity and high droplet adhesion using hydrophobic and hydrophilic nanoparticles. *Journal of Colloid and Interface Science*, 384:182-188, 2012.

[15] Saito, A. Material design and structural color inspired by biomimetic approach. *Science and Technology of Advanced Materials*, 12:064709, 2011.

[16] http://imagej.nih.gov/ij/

[17] Cassie, A. B. D. Contact angles. *Discussions of the Faraday Society*, 3:11-16, 1948.

[18] Wenzel, R. N. Surface Roughness and Contact Angle. *The Journal of Physical Chemistry*, 53:1466-1467, 1949.

[19] Blossey, R. Self-cleaning surfaces — virtual realities. *Nature Materials*, 2:301-306, 2003.

[20] Bhushan, B., Nosonovsky, M. The rose petal effect and the modes of superhydrophobicity. *Philosophical Transactions of the Royal Society A*, 368:4713-4728, 2010.

[21] Pierce, E., Carmona, F. J., Amirfazli, A. Understanding of sliding and contact angle results in tilted plate experiments. *Colloids and Surfaces A: Physicochemical and Engineering Aspects*, 323:73–82, 2008.

22] Bhushan B, Nosonovsky M. The rose petal effect and the modes of superhydrophobicity. *Philosophical Transactions of the Royal Society A*, 368: 4713–4728, 2010.

[23] Bormashenko E, Stein T, Pogreb R, Aurbach D. Petal Effect on Surfaces Based on Lycopodium: High-Stick Surfaces Demonstrating High Apparent Contact Angles. *The Journal of Physical Chemistry C*, 113:5568-5572, 2009.

[24] Schulte A J, Droste D M, Koch K, Barthlott W. Hierarchically structured superhydrophobic flowers with low hysteresis of the wild pansy (Viola tricolor) new design principles for biomimetic materials. *Beilstein Journal of Nanotechnology*, 2:228-36, 2011.

[25] Bhushan B, Jung Y C. Wetting study of patterned surfaces for superhydrophobicity. *Ultramicroscopy*, 107:1033-1041, 2007.

[26] Aideo, S. N., Mohanta, D. Limiting hydrophobic behavior and reflectance response of dragonfly and damselfly wings. *Applied Surface Science*, 387:609-616, 2016.

[27] White, J. A., Santos, M. J., Rodríguez-Valverde, M. A., Velasco, S. Numerical Study of the Most Stable Contact Angle of Drops on Tilted Surfaces. *Langmuir*, 31:5326−5332, 2015.

[28] Kim, D., Pugno, N. M., Ryu, S., Wetting theory for small droplets on textured solid surfaces. *Scientific Reports*, 6:37813, 2016.

[29] Adam, N.K., Livingston, H.K. Contact Angles and Work of Adhesion. *Nature*, 182(4628):128, 1958.

[30] Webb, H. K., Hasan J., Truong, V. K ., Crawford, R. J., Ivanova, E. P. Nature inspired structured surfaces for biomedical applications. *Current medicinal chemistry*, 18: 3367-3375, 2011.

[31] Webb, H. K., Crawford, R. J., Ivanova, E. P., Wettability of natural superhydrophobic surfaces. *Advances in Colloid and Interface Science*, 210:58–64, 2014.

[32] Yeh, K-Yu., Chen, L-Jen. Contact Angle Hysteresis on Regular Pillar-like Hydrophobic Surfaces. *Langmuir*, 24:245-251, 2008.

[33] Whitney, H. M., Kolle, M., Andrew, P., Chittka, L., Steiner, U., Glover, B. J. Floral iridescence, produced by diffractive optics, acts as a cue for animal pollinators. *Science*, 323:130-133, 2009

[34] CIE (1932). *Commission internationale de l'Eclairage proceedings, 1931*. Cambridge: Cambridge University Press, UK.

[35] Aideo, S. N., Haloi, R., Mohanta, D. Exploring structural colour in uni- and multi-coloured butterfly wings and $Ag^{+}$ uptake by scales. *Europhysics Letters*, 119:66003-1-7, 2017.